

Coherent Curvature Radiation Spectrum by Dynamically Fluctuating Bunches in Magnetospheres

Yuan-Pei Yang^{1,2*} and Bing Zhang^{3,4†}

¹South-Western Institute for Astronomy Research, Yunnan University, Kunming, Yunnan 650504, People's Republic of China

²Purple Mountain Observatory, Chinese Academy of Sciences, Nanjing, Jiangsu 210023, People's Republic of China

³Nevada Center for Astrophysics, University of Nevada, Las Vegas, NV 89154, USA

⁴Department of Physics and Astronomy, University of Nevada, Las Vegas, NV 89154, USA

Accepted XXX. Received YYY; in original form ZZZ

ABSTRACT

Coherent curvature radiation by charged bunches has been discussed as the radiation mechanism for radio pulsars and fast radio bursts. Important issues for this radiation mechanism include how the bunches form and disperse in the magnetosphere of a pulsar or magnetar. More likely, bunches form and disperse continuously and it remains unclear what the spectral features are for these fluctuating bunches. In this work, we consider that the bunches in a magnetosphere have a formation rate of λ_B , a lifetime of τ_B , and a typical Lorentz factor of γ , and analyze the spectral features of coherent curvature radiation by these fluctuating bunches. We find that the emission spectrum by a single fluctuating bunch is suppressed by a factor of $\sim (\lambda_B \tau_B)^2$ compared with that of a single persistent bunch, and there is a quasi-white noise in a wider band in the frequency domain. The high-frequency cutoff of the spectrum is at $\sim \max(\omega_{\text{peak}}, 2\gamma^2/\tau_B)$, where ω_{peak} is the peak frequency of curvature radiation. If the observed spectrum is not white-noise-like, the condition of $2\gamma^2 \lambda_B \gtrsim \min(\omega_{\text{peak}}, 2\gamma^2/\tau_B)$ would be required. Besides, the radiation by multiple fluctuating bunches along a field line is the incoherent summation of the radiation by single bunches if the bunch separation is longer than the wavelength. Conversely, a coherent summation should be involved. We also discuss the effects of bunch structures and the mechanism of bunch formation and dispersion.

Key words:

radiation mechanisms: non-thermal – radio continuum: general – (transients:) fast radio bursts – (stars:) pulsars: general

1 INTRODUCTION

The brightness temperatures of both radio pulsars and fast radio bursts (FRBs) are extremely high and are much greater than any plausible thermal temperature of the emitting electrons (e.g., Melrose 2017; Petroff et al. 2019; Cordes & Chatterjee 2019; Zhang 2020, 2022a; Xiao et al. 2021; Lyubarsky 2021; Bailes 2022). This suggests that the radiation mechanism of radio pulsars and FRBs must be coherent. For incoherent waves with random phases, the amplitude square of their superposition is approximately the sum of the amplitude squares of each wave. Thus, the observed emission power would be the simple summation of the emission power of individual charged particles, as proposed in most astrophysical scenarios. For coherent waves with certain phase differences, the amplitude square of their superposition could be significantly enhanced or reduced due to the wave coherent superposition process. In particular, “coherently enhanced” waves usually require that the phase differences of superposing waves must be much less the half wavelength of the waves. In the literature about radiation mechanism, “coherent” is mainly defined as “coherently enhanced”.

Some coherent emission mechanisms have been invoked to interpret the emissions of radio pulsars and FRBs (e.g., Melrose 2017; Zhang 2022a): coherent radiation by charged bunches (i.e., antenna mechanism), maser by hydrodynamic instabilities or kinetic instabilities, etc. In this paper, we mainly focus on coherent curvature radiation by charged bunches that have been proposed as one of the popular ideas to explain the emission of pulsars (Sturrock 1971; Ginzburg & Zhelezniakov 1975; Ruderman & Sutherland 1975; Buschauer & Benford 1976; Benford & Buschauer 1977; Asseo & Melikidze 1998; Melikidze et al. 2000; Gil et al. 2004; Basu et al. 2022; Rahaman et al. 2022) and FRBs (Katz 2014, 2018; Kumar et al. 2017; Lu & Kumar 2018; Yang & Zhang 2018b; Kumar & Bošnjak 2020; Lu et al. 2020; Yang et al. 2020; Cooper & Wijers 2021; Wang et al. 2022a,b; Tong & Wang 2022; Liu et al. 2022; Qu et al. 2023). Due to the two-stream instabilities in the magnetosphere of a neutron star, charged bunches might form and radiate electromagnetic radiation coherently (Ruderman 1971; Benford & Buschauer 1977; Cheng & Ruderman 1977; Usov 1987; Rahaman et al. 2020; Kumar et al. 2022). However, as pointed out by some authors (e.g., Melrose 2017; Lyubarsky 2021), these models involving charged bunches have some important issues: (1) The charged bunches might be short-lived; (2) The radiation might be strongly suppressed by the magnetosphere plasma. For the latter issue, Gil et al. (2004) and Lyubarsky (2021) pointed out that electromagnetic waves with frequencies below the

* E-mail: ypyang@ynu.edu.cn (YPY)

† E-mail: bing.zhang@unlv.edu (BZ)

plasma frequency could propagate in the highly magnetized plasma in the magnetosphere, but the radiation power would be significantly suppressed. However, [Qu et al. \(2023\)](#) recently found that the plasma suppression effect could be ignored in the case of FRBs because of the existence of a parallel electric field in the FRB emission region, as is required to power the bright FRB emission. The former issue leads to a more fundamental question: Is it necessary that the charged bunches have to be long-lived in order to explain the observed features of radio pulsars and FRBs? In other words, how do the formation and dispersion of bunches affect the observed radiation?

In this work, we will analyze the spectral features of the coherent curvature radiation by dynamically fluctuating bunches in the magnetosphere of a neutron star. We consider that the bunches in the magnetosphere form with an average rate of λ_B and have an average lifetime of τ_B , and discuss how λ_B and τ_B affect the radiation spectral feature. The paper is organized as follows. In Section 2, we discuss the brightness temperature of curvature radiation in a magnetosphere using a more physical treatment. In Section 3, we analyze the spectral features of coherent curvature radiation by fluctuating bunches, including the features by a single persistent bunch with different structures (Section 3.1), a single fluctuating bunch (Section 3.2), and multiple fluctuating bunches (Section 3.3). In Section 4, we discuss the formation and dispersion mechanisms of bunches in the magnetosphere and calculate λ_B and τ_B . The results are summarized and discussed in Section 5. The convention $Q_x = Q/10^x$ is adopted in cgs units unless otherwise specified.

2 BRIGHTNESS TEMPERATURE: THE DIFFERENCE BETWEEN OBSERVATIONAL TREATMENT AND PHYSICAL TREATMENT

Before discussing the spectral features of coherent curvature radiation by charged bunches, we point out the differences between the observational treatment and the physical treatment of brightness temperature. The observational brightness temperature is usually defined by

$$T_B = \frac{1}{2\pi k_B} \left(\frac{d}{v\Delta t} \right)^2 F_\nu = 10^{35} \text{ K } d_{\text{Gpc}}^2 v_9^{-2} \Delta t_{-3}^{-2} F_{\nu, \text{Jy}}, \quad (1)$$

where k_B is the Boltzmann constant, d is the distance between source and observer¹, Δt is the duration of a transient, v is the frequency of the electromagnetic wave, $d_{\text{Gpc}} = d/1 \text{ Gpc}$ and $F_{\nu, \text{Jy}} = F_\nu/1 \text{ Jy}$. Since all quantities in Eq.(1) are observable, this brightness temperature could be directly estimated from the observations (e.g., [Xiao & Dai 2022](#); [Luo et al. 2023](#); [Zhu-Ge et al. 2023](#)). However, this observationally-defined brightness temperature is based on a toy model that the transverse size of the emission region is approximately $c\Delta t$, which does not apply to broader astrophysical scenarios, which we discuss more below.

We first briefly summarize the meaning of the physical brightness temperature. For a photon field within a volume element dV and a solid angle element $d\Omega$, the number of states per volume per frequency interval per solid angle is given by (e.g., [Rybicki & Lightman 1986](#))

$$dN_s = \frac{2dVd^3k}{(2\pi)^3} = \frac{2v^2}{c^3} dVdv d\Omega, \quad (2)$$

¹ Here we do not specify whether d is luminosity distance or angular diameter distance for an order of magnitude estimate. A more precise treatment involves a correction factor with a certain power of $(1+z)$, see [Luo et al. \(2023\)](#) and [Zhang \(2022a\)](#) for details.

where $d^3k = k^2 dk d\Omega$ is the three-dimensional wave vector element, and the factor 2 accounts for the fact that photons have two independent polarizations per wave vector \vec{k} . As bosons, the average number of photons in a state, i.e. the occupation number, is

$$\mathcal{N} = \frac{1}{\exp(hv/kT) - 1}, \quad (3)$$

where T is the temperature of the photon field. Therefore, the directional energy density $u_\nu(\Omega)$ is given by

$$u_\nu(\Omega) dV dv d\Omega = \frac{2v^2}{c^3} hv \mathcal{N} dV dv d\Omega. \quad (4)$$

For radio observations, the brightness temperature T_B is usually defined under the Rayleigh-Jeans limit, $I_\nu = 2v^2 k T_B / c^2$. Using $u_\nu(\Omega) = I_\nu / c$, one finally has

$$kT_B = \mathcal{N} hv. \quad (5)$$

Thus, *the brightness temperature directly reflects the photon energy per state*. The physical implications of an extremely large brightness temperature include the following: (1) For incoherent radiation, there is a maximum brightness temperature a gas can reach without undergoing Compton catastrophe (e.g., [Longair 2011](#); [Melrose 2017](#)), and for a synchrotron self-absorbed radio source, this maximum brightness temperature is $\sim 10^{12} \text{ K}$; (2) Induced Compton scattering would be significant at a high brightness temperature because photons satisfy Bose-Einstein statistics (e.g., [Lyubarsky & Ostrovska 2016](#); [Lu & Kumar 2018](#)); (3) The interaction between electromagnetic waves and particles/plasmas in the ambient medium would be non-linear due to the particles' relativistic motion in strong electromagnetic waves (e.g., [Yang & Zhang 2020](#)).

Physically, the flux-intensity relation is generally given by $F_\nu = \pi I_\nu (l_e/d)^2$, where l_e is the emission region transverse scale perpendicular to the line of sight. The brightness temperature can be therefore written as

$$T_B = \frac{c^2}{2\pi k_B v^2} \left(\frac{d}{l_e} \right)^2 F_\nu. \quad (6)$$

This equation can be reduced to the observationally defined brightness temperature Eq.(1) when $l_e = c\Delta t$ is satisfied. For this equation to be satisfied, three conditions are needed: (1) The emission region is non-relativistic; (2) Its longitudinal scale is the same order of magnitude as the transverse scale; (3) The radiation is isotropic at any point in the emission region.

In realistic physical conditions, the transverse scale l_e is model dependent and could be different from $c\Delta t$. The physical brightness temperature could be very different within different physical scenarios given the same observations. A well-known effect that has been discussed in the literature is when the emitter has a relativistic bulk motion, e.g. within the scenarios invoking a relativistic outflow (e.g., [Lyubarsky 2014](#); [Beloborodov 2017](#); [Metzger et al. 2017](#)). The above-mentioned condition 1 and condition 2 would not be satisfied. The transverse scale of the emission region l_e is about $l_e \approx 2\Gamma^2 c\Delta t / \Gamma = 2\Gamma c\Delta t$, where Γ is the Lorentz factor of the outflow. Due to relativistic motion, the observable emission region of the outflow is within the angle of $1/\Gamma$ pointing to the observer. Then the physical brightness temperature is

$$T_B = \frac{1}{8\pi k_B} \left(\frac{d}{v\Gamma\Delta t} \right)^2 F_\nu = 2.7 \times 10^{32} \text{ K } d_{\text{Gpc}}^2 v_9^{-2} \Delta t_{-3}^{-2} \Gamma_1^{-2} F_{\nu, \text{Jy}}, \quad (7)$$

which is much smaller than that given by the traditional formula in Eq.(1).

Here we point out that the physical brightness temperature in magnetospheric models, including the curvature radiation scenario discussed in this paper, is also different from the traditional definition and should be properly redefined.

We consider the case that the emission region is within a magnetosphere and charged particles are moving relativistically, as are envisaged in many theoretical models of radio pulsars and FRBs (e.g., Sturrock 1971; Ruderman & Sutherland 1975; Kumar et al. 2017; Yang & Zhang 2018b; Lu et al. 2020). The above-mentioned condition (2) and (3) would not be satisfied. We consider that the charged particles/bunches are relativistically moving with a Lorentz factor γ along the curved field lines with a curvature radius ρ . For $\omega \gtrsim \omega_c$, where $\omega_c \sim \gamma^3 c/\rho$ is the typical frequency of curvature radiation, the radiation beaming angle at the angular frequency ω is approximately (Jackson 1998)

$$\theta_e(\omega) \sim \frac{1}{\gamma} \left(\frac{\omega_c}{\omega} \right)^{1/3}, \quad (8)$$

which involves the field line direction. Thus, the transverse length-scale l_e of the emission region at the distance r from the neutron star center should be estimated by

$$\begin{aligned} l_e &\sim r\theta_e(\omega) \sim \frac{3}{4}\rho\theta\theta_e(\omega) \\ &\sim \frac{3}{4}\theta \left(\frac{c\rho^2}{\omega} \right)^{1/3} \approx 2.7 \times 10^5 \text{ cm } \rho_8^{2/3} v_9^{-1/3} \theta, \end{aligned} \quad (9)$$

where $\rho \approx 4r/3\theta$ is the curvature radius at the position (r, θ) , and θ is the poloidal angle between the emission region and the magnetic axis. We can see that for the above typical parameters, the transverse lengthscale l_e is much smaller than that estimated by $c\Delta t \sim 3 \times 10^7 \text{ cm } \Delta t_{-3}$. As a result, a more physical brightness temperature for the curvature radiation can be estimated as

$$\begin{aligned} T_B &= \frac{32\pi}{9k_B} \left(\frac{d}{\theta} \right)^2 \left(\frac{c}{\rho\omega} \right)^{4/3} F_\nu \\ &= 1.3 \times 10^{39} \text{ K } d_{\text{Gpc}}^2 \theta^{-2} \rho_8^{-4/3} v_9^{-4/3} F_{\nu, \text{Jy}}. \end{aligned} \quad (10)$$

One can see that for curvature radiation in a magnetosphere, the physical brightness temperature should depend on the emission region parameters (ρ, θ) . For typical parameters, the brightness temperature is much larger than the value estimated by the traditional formula Eq.(1). Meanwhile, it is worth noting that such a brightness temperature is independent of the burst duration Δt . The reason is that the burst duration does not directly reflect the transverse size of the emission region.

3 COHERENT CURVATURE RADIATION BY FLUCTUATING BUNCHES

In the magnetosphere of a neutron star, charged bunches form and disperse continuously. Charged bunches are thought to be formed by certain plasma instabilities in the magnetosphere, e.g., two-stream instability (Ruderman & Sutherland 1975; Benford & Buschauer 1977; Cheng & Ruderman 1977; Usov 1987; Asseo & Melikidze 1998; Melikidze et al. 2000; Rahaman et al. 2020), and be dispersed by electrostatic repulsion, velocity dispersion, etc. In this section, we mainly calculate the spectrum of the coherent curvature radiation by fluctuating bunches and discuss how the spectral feature is affected by the bunch formation and dispersion.

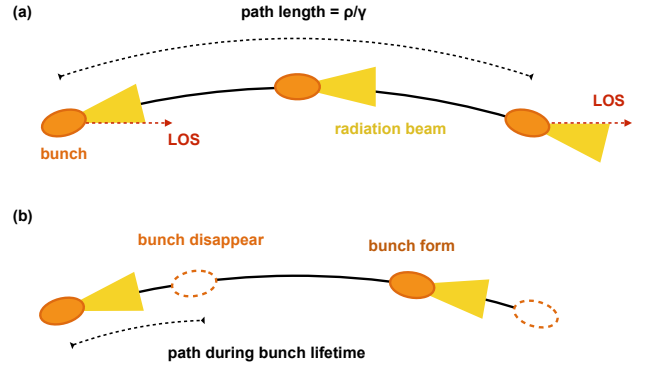


Figure 1. Schematic configurations of a bunch moving along a magnetic field line and emitting curvature radiation. The black line denotes the magnetic field line, the orange ellipse denotes the bunch, the dashed ellipse denotes the bunch disappearing due to dispersion, and the yellow region denotes the radiation by the bunch due to relativistic motion. Panel (a): the bunch is persistent. Due to the relativistic motion of the bunch, the length scale of the path along the line of sight (LOS) is ρ/γ , where ρ is the curvature radius of the field line, and γ is the bunch Lorentz factor. (b) the bunch is fluctuating due to rapid formation and dispersion when the building plasma moves along the field line.

3.1 Radiation by a single persistent bunch with different structures

First, we briefly summarize the spectral properties of a single persistent bunch. We consider that the bunch has the velocity v with Lorentz factor $\gamma = (1 - v^2/c^2)^{-1/2}$ and moves along the magnetic field line with a curvature radius ρ , as shown in the panel (a) of Figure 1.

If the bunch lifetime is long enough, $\tau_B > \rho/\gamma c$, which is comparable to the time of a persistent bunch sliding along a curved magnetic field line, the observer will see the radiation with the emission cone of angular width $\sim 1/\gamma$ around the observer direction, and the typical angular frequency of the emission wave is

$$\omega_c = \frac{1}{\tau_c} \sim \left[\frac{\rho}{\gamma c} \left(1 - \frac{v}{c} \right) \right]^{-1} \approx \frac{2\gamma^3 c}{\rho}, \quad (11)$$

where τ_c is the typical pulse duration of the classical curvature radiation for a single point source, and the factor of $(1 - v/c)$ is due to the propagation time-delay effect.

We consider that the classical curvature radiation is in the form of a finite pulse $E(t)$, and $E(t)$ vanishes sufficiently rapidly for $t \rightarrow \pm\infty$. For convenience, we define $A(t) \equiv (c/4\pi)^{1/2} [RE(t)]_{\text{ret}}$, where R is the distance between the observer and the bunch at the retarded time, and the bracket $[\dots]_{\text{ret}}$ is evaluated at the retarded time. The Fourier transform of $A(t)$ is defined as

$$A(\omega) = \frac{1}{\sqrt{2\pi}} \int_{-\infty}^{\infty} A(t) e^{i\omega t} dt, \quad (12)$$

$$A(t) = \frac{1}{\sqrt{2\pi}} \int_{-\infty}^{\infty} A(\omega) e^{-i\omega t} d\omega. \quad (13)$$

Here we adopt the above definitions of Fourier transforms as the same as those in Jackson (1998), and the corresponding properties of Fourier transform will be adopted accordingly in the following discussion. The directional emission spectrum (defined as the radiation energy per unit solid angle per unit angular frequency) is (Jackson

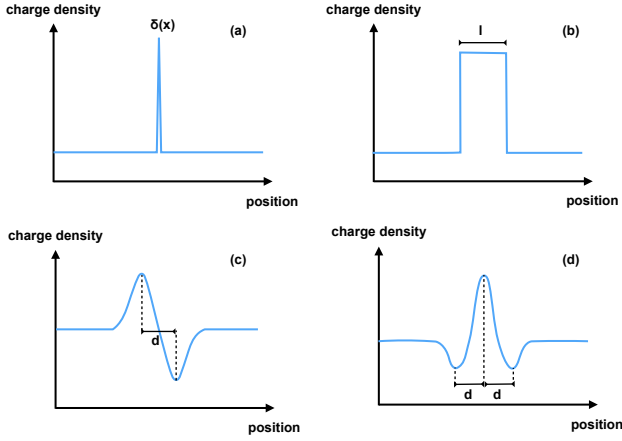


Figure 2. Charge density distributions for different bunch structures. Panel (a): A single point-source bunch, with the charge density described by a delta function $\delta(x)$; Panel (b): A one-dimensional bunch with lengthscale l , with a uniform charge density; Panel (c): A bunch-cavity pair formed in a plasma background, with the separation between the bunch and the cavity being d . Panel (d): A bunch-cavity system satisfying the structures of a soliton, with the separations between the bunch and the cavities being d .

1998)

$$P_A(\omega) \equiv \frac{dW}{d\Omega d\omega} = 2|A(\omega)|^2 = \frac{c}{4\pi^2} \left| \int_{-\infty}^{\infty} [RE(t)]_{\text{ret}} e^{i\omega t} dt \right|^2. \quad (14)$$

For the curvature radiation by a single persistent bunch, the properties of $P_A(\omega)$ mainly depend on the spatial structure of the charged bunch (Yang & Zhang 2018b; Yang et al. 2020). We briefly summarize the following three scenarios with the different structures as shown in Figure 2:

1. A point-source bunch (see the panel (a) of Figure 2): If the bunch length is much smaller than a half wavelength, the point-source approximation is reasonable. The emission spectrum of the curvature radiation is (Jackson 1998; Yang & Zhang 2018b)

$$P_A(\omega) \propto \omega^{2/3} e^{-\omega/\omega_c}. \quad (15)$$

In particular, the spectral index of $2/3$ is due to the angular spectrum involved in the curvature radiation, which is different from the scenario of synchrotron radiation that is usually described by total spectrum with a spectral index of $1/3$, except the case with a narrow pitch-angle distribution (Yang & Zhang 2018a). The emission spectrum is shown by the black curve in Figure 3.

2. A one-dimensional bunch with a finite length l (see the panel (b) of Figure 2): The corresponding emission spectrum of curvature radiation is (Yang & Zhang 2018b)

$$P_A(\omega) \propto \text{sinc}^2\left(\frac{\omega}{\omega_l}\right) \omega^{2/3} e^{-\omega/\omega_c} \quad \text{with } \omega_l \simeq 2c/l, \quad (16)$$

where $\text{sinc}(x) \equiv \sin x/x$ that is involved due to the coherent summation of the phase factor of the charged particles at different regions on the one-dimensional bunch (also see the similar derivation of Eq.(55)), ω_l is the angular frequency corresponding to the half length of a bunch. Here the charge distribution of the bunch is assumed to be uniform. If $\omega \gg \omega_l$, one has $\text{sinc}^2(\omega/\omega_l) \sim \omega^{-2}$ due to the rapid oscillation of the term $\sin^2(\omega/\omega_l)$ with a unit amplitude in the sinc function, leading to a softer spectrum compared with that of a point source. The emission spectrum is shown by the red curve

in Figure 3. In particular, when $\omega_l < \omega_c$, the peak radiation specific power would be suppressed by a factor of $\sim (\omega_l/\omega_c)^{2/3}$, leading to the total radiation energy suppressed by a factor

$$\eta_l \simeq \frac{\omega_l P_A(\omega_l)}{\omega_c P_A(\omega_c)} \simeq \left(\frac{\omega_l}{\omega_c}\right)^{5/3} \simeq 0.9 I_1^{-5/3} v_{c,9}^{-5/3}, \quad (17)$$

compared with that of a point source given by Eq.(15). This formula can be used to estimate how the bunch length suppresses the total radiation power.

3. A bunch-cavity pair or similar system formed by plasma background fluctuation (see panel (c) and panel (d) of Figure 2). First, we consider that a charged bunch forms in the plasma background and has a charge density larger than the background, then a corresponding cavity with a charge density smaller than the background would form near the bunch, as shown in panel (c) of Figure 2. For simplicity, we treat the bunch-cavity pair as a two-point source with a separation d . Thus, the charge density distribution of the bunch-cavity pair system could be described by $\rho_{bc}(x) = q\delta(x) - q\delta(x-d) + \rho_0$, where x denotes the pair position, $\pm q$ in the first two terms correspond to the charges of the bunch and the cavity, respectively, and ρ_0 is the charge density of the plasma background. Since a persistent current (i.e., plasma background) cannot generate electromagnetic waves (Yang & Zhang 2018b), only the first two terms contribute to the radiation. Therefore, the radiation of the bunch-cavity pair is consistent with that of a separated electron/positron pair discussed by Yang et al. (2020). Based on the charge density distribution, the pulse profile is given by $A(t) = A_0(t) - A_0(t-d/c)$, where $A_0(t)$ and $-A_0(t-d/c)$ correspond to the pulse profiles of the bunch and the cavity, respectively. According to the time-shifting property of the Fourier transform, one has $A(\omega) = A_0(\omega) - A_0(\omega)e^{i\omega d/c}$. Using Eq.(15) and $P_A(\omega) = 2|A(\omega)|^2$ by Eq.(14), one has (also see Yang et al. 2020)

$$P_A(\omega) \propto 4 \sin^2\left(\frac{\omega}{\omega_d}\right) \omega^{2/3} e^{-\omega/\omega_c} \quad \text{with } \omega_d \simeq 2c/d. \quad (18)$$

For $\omega \ll \omega_d$, one has $\sin^2(\omega/\omega_d) \propto \omega^2$, leading to $P_A(\omega) \propto \omega^{8/3}$ at the low-frequency band. Thus, the radiation spectrum is much narrower and harder than that of a point source given by Eq.(15). The emission spectrum is shown by the blue curve in Figure 3. Furthermore, it can be further proved that the above formula is also available for some more complex bunch-cavity systems. For example, Melikidze et al. (2000) proposed that some plasma solitons with net charges will result from a ponderomotive Miller force. Each soliton consists of one large bunch and two small cavities (see Figure 2 in Melikidze et al. (2000) and panel (d) of Figure 2), because the excess of one charge is compensated by the lack of this charge in the nearby regions. The charge density distribution of the bunch-cavity system could be roughly described by $\rho_{bc}(x) = -q\delta(x-d) + 2q\delta(x) - q\delta(x+d) + \rho_0$. Similar to the calculation of the bunch-cavity pair, the same result as Eq.(18) is obtained, as shown by the blue curve in Figure 3.

The above discussion assumes that the particles in the bunch have a Lorentz factor γ . If the energy distribution of the charged particles satisfies a power-law distribution, the corresponding radiation spectrum would be characterized by a multi-segment broken power-law, and the details have been discussed by Yang & Zhang (2018b).

3.2 Radiation by a single fluctuating bunch

If the bunch lifetime is short, $\tau_B < \rho/\gamma c$, the observed pulse duration will be shorter than τ_c given by Eq.(11), leading to a higher typical

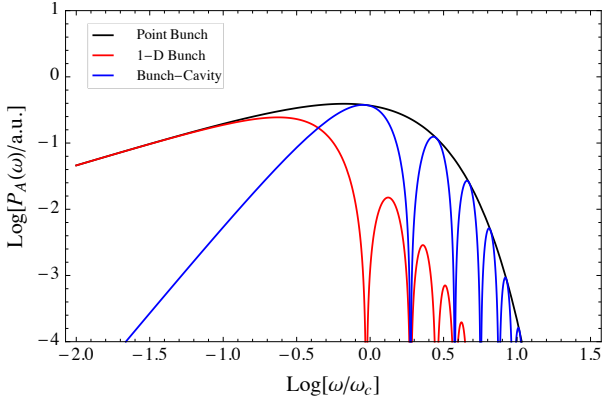


Figure 3. The emission spectrum of a single persistent bunch. The black, red, and blue curves correspond to the emission spectrum of a point-source bunch (panel (a) in Figure 2), a one-dimensional bunch with $\omega_l = 0.3\omega_c$ (panel (b) in Figure 2), a bunch-cavity system (a bunch-cavity pair (panel (c) in Figure 2) or a soliton (panel (d) in Figure 2) with $\omega_d = 0.3\omega_c$, respectively. The unit of the emission spectrum is arbitrary. For easy comparison with the spectral shapes of different scenarios, the emission spectrum of the bunch-cavity system is suppressed by an arbitrary factor in this figure.

frequency than that of classical curvature radiation, i.e.

$$\tilde{\omega}_c \sim \left[\tau_B \left(1 - \frac{v}{c} \right) \right]^{-1} \sim \frac{2\gamma^2}{\tau_B}. \quad (19)$$

A fluctuating bunch with a short lifetime will generate electromagnetic radiation with a higher frequency than the typical frequency of classical curvature radiation.

We consider that a bunch forms and disperses intermittently when the building particles move along a field line, and the coherent radiation pulses are generated when the bunch exists, as shown in panel (b) of Figure 1. The bunch forms with a rate of λ_B and disperses during a lifetime of τ_B . Due to the relativistic motion of the building particles with $\gamma \gg 1$, the pulse rate λ_b and the pulse duration τ_b should be corrected by the propagation time-delay effect, i.e.

$$\lambda_b = \left(1 - \frac{v}{c} \right)^{-1} \lambda_B \approx 2\gamma^2 \lambda_B, \quad (20)$$

$$\tau_b = \left(1 - \frac{v}{c} \right) \tau_B \approx \frac{\tau_B}{2\gamma^2} \sim \tilde{\omega}_c^{-1}, \quad (21)$$

where the factor of $(1 - v/c)$ is due to the propagation time-delay effect.

During the time of $\rho/\gamma c$ when the emission cone sweeps the observing direction, the bunch would disperse and generate multiple times when the building plasma particles move along the magnetic field line. We consider that the radiation is in the form of $\tilde{A}(t)$. When the bunch exists, $\tilde{A}(t) \approx A(t)$, where $A(t)$ is the radiation form of the classical curvature radiation by a single persistent source, as discussed in Section 3.1; when the bunch disappears, $\tilde{A}(t) \approx 0$. Therefore, the form of $\tilde{A}(t)$ can be written as

$$\tilde{A}(t) = A(t)S(t), \quad (22)$$

where $S(t)$ is the pulse sampling function with

$$S(t) = \begin{cases} 1 & \text{for bunch existing,} \\ 0 & \text{for bunch disappearing,} \end{cases} \\ = \sum_k s(t - t_k), \quad (23)$$

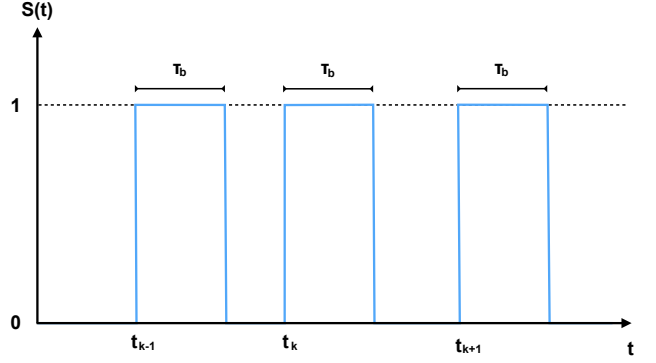


Figure 4. The pulse sampling function $S(t)$ given by Eq.(23). $\{t_k\}$ is the starting time of the k -th pulse. Each pulse has a duration of τ_b .

and

$$s(t) = \begin{cases} 1 & \text{for } 0 \leq t \leq \tau_b, \\ 0 & \text{for otherwise.} \end{cases} \quad (24)$$

Here t_k corresponds to the starting time of the k -th generation of the bunch, and τ_b is the pulse duration of the radiation from a bunch. The pulse sampling function $S(t)$ is shown in Figure 4.

We assume that pulse generation satisfies a Poisson process, thus, the probability to generate k pulses during time t is

$$P_k(t) = \frac{(\lambda_b t)^k}{k!} e^{-\lambda_b t}, \quad (25)$$

where $\lambda_b = 2\gamma^2 \lambda_B$ is the pulse rate that is corrected for the propagation time-delay effect. Here $\{t_k\}$ in Eq.(23) is distributed in a Poisson distribution with the parameter λ_b , and the probability density function of $\{t_k\}$ is related to the probability that the k -th point occurs in a short interval at the arbitrary time t for short Δt ,

$$p_{t_k}(t)\Delta t = P(t < t_k < t + \Delta t) \\ = P_{k-1}(t)P_1(\Delta t) = P_{k-1}(t)\lambda_b \Delta t. \quad (26)$$

Thus, one obtains the probability density function for $\{t_k\}$, i.e.

$$p_{t_k}(t) = \lambda_b P_{k-1}(t). \quad (27)$$

Before calculating the emission spectrum $P_{\tilde{A}}(\omega)$ of $\tilde{A}(t)$, we are first interested in its autocorrelation function $R_{\tilde{A}}(\tau)$. Since $S(t)$ corresponds to a random sampling process, $R_{\tilde{A}}(\tau)$ could be described by

$$R_{\tilde{A}}(\tau) = \mathcal{E} \left[\tilde{A}(t) * \tilde{A}^\dagger(-t) \right] = \mathcal{E} \left[(A(t)S(t)) * (A(-t)S(-t))^\dagger \right] \\ = \mathcal{E} \left[\int_{-\infty}^{\infty} A(t + \tau)S(t + \tau)A^\dagger(t)S^\dagger(t)dt \right] \\ = \int_{-\infty}^{\infty} A(t + \tau)A^\dagger(t)\mathcal{E} \left[S(t + \tau)S^\dagger(t) \right] dt, \quad (28)$$

where $\tilde{A}(t) * \tilde{A}^\dagger(-t)$ denotes the autocorrelation function of $\tilde{A}(t)$, and $\mathcal{E}[X]$ denotes the expectation of the random variable X involved by the random process. The symbol “*” denotes the convolution operator, and the superscript “ \dagger ” denotes the conjugation operator. In the above calculation, the property of $\int_{-\infty}^{\infty} f(t)f^\dagger(t - \tau)dt = \int_{-\infty}^{\infty} f(t + \tau)f^\dagger(t)dt$ is used based on variable substitution $t - \tau \rightarrow t$. For the Poisson sampling process, the autocorrelation of $R_S(\tau)$

satisfies (Franks 1981)

$$\begin{aligned}
R_S(\tau) &= \mathcal{E} \left[S(t+\tau)S^\dagger(t) \right] = \sum_k \sum_j \mathcal{E} \left[s(t+\tau-t_k)s(t-t_j) \right] \\
&= \sum_{k=j} \int_{-\infty}^{\infty} s(t+\tau-\xi)s(t-\xi)p_{t_k}(\xi)d\xi \\
&+ \sum_{k \neq j} \int_{-\infty}^{\infty} s(t+\tau-\eta)p_{t_k}(\eta)d\eta \int_{-\infty}^{\infty} s(t-\sigma)p_{t_k}(\sigma)d\sigma \\
&= (\lambda_b q_s)^2 + \lambda_b r_s(\tau), \tag{29}
\end{aligned}$$

where

$$q_s \equiv \int_{-\infty}^{\infty} s(t)dt, \tag{30}$$

$$r_s(\tau) \equiv \int_{-\infty}^{\infty} s(t+\tau)s(t)dt. \tag{31}$$

Notice that both $S(t)$ and $s(t)$ are real functions according to Eq.(23) and Eq.(24). Since the autocorrelation function $R_S(\tau)$ is independent of t (i.e., a wide-sense-stationary process), Eq.(28) could be finally written as

$$R_{\tilde{A}}(\tau) = R_A(\tau)R_S(\tau), \tag{32}$$

where $R_A(\tau)$ is the autocorrelation function of $A(t)$. Therefore, the autocorrelation function of the product of $A(t)$ and $S(t)$ is the product of the autocorrelation of each one.

The emission spectrum of $\tilde{A}(t)$ is given by Eq.(14),

$$P_{\tilde{A}}(\omega) \equiv \frac{d\tilde{W}}{d\Omega d\omega} = 2|\tilde{A}(\omega)|^2. \tag{33}$$

According to the convolution theorem and conjugation property of the Fourier transform, $|\tilde{A}(\omega)|^2$ could be written as

$$\begin{aligned}
|\tilde{A}(\omega)|^2 &= \tilde{A}(\omega)\tilde{A}^\dagger(\omega) \\
&= \frac{1}{\sqrt{2\pi}}\mathcal{F}(\tilde{A}(t) * \tilde{A}^\dagger(-t)) = \frac{1}{\sqrt{2\pi}}\mathcal{F}(R_{\tilde{A}}(\tau)), \tag{34}
\end{aligned}$$

where $\mathcal{F}(\dots)$ denotes the Fourier transform, the factor of $1/\sqrt{2\pi}$ is involved due to the definition of Fourier transform Eq.(12) and Eq.(13). Thus, the Fourier transform of the autocorrelation function is the power spectrum, known as the Wiener-Khinchin's theorem. According to Eq.(32), Eq.(33), Eq.(34) and the convolution theorem, the emission spectrum of $\tilde{A}(t)$ could be finally written as

$$\begin{aligned}
P_{\tilde{A}}(\omega) &= \frac{2}{\sqrt{2\pi}}\mathcal{F}(R_A(\tau)R_S(\tau)) = 2|A(\omega)|^2 * \frac{1}{\sqrt{2\pi}}\mathcal{F}(R_S(\tau)) \\
&= P_A(\omega) * P_S(\omega), \tag{35}
\end{aligned}$$

where $\mathcal{F}(R_A(\tau)R_S(\tau)) = (1/\sqrt{2\pi})\mathcal{F}(R_A(\tau)) * \mathcal{F}(R_S(\tau))$ is used, and the emission spectrum of the pulse sampling function $S(t)$ is defined as

$$P_S(\omega) \equiv \frac{1}{\sqrt{2\pi}}\mathcal{F}(R_S(\tau)). \tag{36}$$

Equation (35) is the most important formula in this section, and we will use it to analyze the spectral features of the coherent radiation by fluctuating bunches. In the following discussion, we will discuss two mathematical models of the pulse sampling profile $S(t)$: impulsive sampling profile and rectangular sampling profile.

3.2.1 Impulsive sampling profile

If the pulse duration τ_b is much shorter than λ_b^{-1} , i.e., $\tau_b \lambda_b \ll 1$, the pulse profile $s(t)$ in Eq.(24) can be well described using the

delta function $\delta(t)$, $s(t) \simeq \tau_b \delta(t)$ for $\tau_b \rightarrow 0$. According to Eq.(30) and Eq.(31), one has $r_s \simeq \tau_b^2 \delta(\tau)$ and $q_s \simeq \tau_b$. Using Eq.(23) and Eq.(29), the autocorrelation function $R_S(\tau)$ of $S(t)$ is

$$R_S(\tau) = (\lambda_b \tau_b)^2 + \lambda_b \tau_b^2 \delta(\tau). \tag{37}$$

According to Eq.(36), the emission spectrum of $S(t)$ is

$$P_S(\omega) = (\lambda_b \tau_b)^2 \delta(\omega) + \frac{\lambda_b \tau_b^2}{2\pi}. \tag{38}$$

Based on Eq.(35), the emission spectrum of $\tilde{A}(t)$ is

$$P_{\tilde{A}}(\omega) = P_A(\omega) * P_S(\omega) = (\lambda_b \tau_b)^2 P_A(\omega) + \frac{\lambda_b \tau_b^2}{2\pi} P_{A,\text{tot}}, \tag{39}$$

where $P_{A,\text{tot}}$ is the total radiation energy of $A(t)$,

$$P_{A,\text{tot}} = \int_{-\infty}^{\infty} P_A(\omega)d\omega. \tag{40}$$

Compared with that of a persistent bunch, $P_A(\omega)$, the emission spectrum of a fluctuating bunch is suppressed by a factor of $\sim (\lambda_b \tau_b)^2 = (\lambda_B \tau_B)^2$. For the scenario of an impulsive sampling profile, $\lambda_b \tau_b \ll 1$ has been potentially assumed. Meanwhile, the emission spectrum of a single fluctuating bunch is the sum of the emission spectrum of a persistent bunch and a white noise that is independent of frequency ω . The ‘‘signal-to-noise ratio’’ at the peak frequency ω_{peak} in the frequency domain is given by

$$\left. \frac{S}{N} \right|_{\text{peak}} \simeq \frac{(\lambda_b \tau_b)^2 P_A(\omega_{\text{peak}})}{(\lambda_b \tau_b^2 / 2\pi) P_{A,\text{tot}}} \simeq \frac{2\pi \lambda_b}{\omega_{\text{peak}}}, \tag{41}$$

where $P_{A,\text{tot}} \sim \omega_{\text{peak}} P_A(\omega_{\text{peak}})$ is adopted based on the wide spectrum property of the curvature radiation. We can see that $(S/N)_{\text{peak}}$ is independent of τ_b , and the larger the pulse rate λ_b , the larger $(S/N)_{\text{peak}}$. The spectrum $P_A(\omega)$ and its peak frequency ω_{peak} depend on the spatial structure of the charged bunch as discussed in Section 3.1. For example: (1) If the bunch is a point-source, $P_A(\omega)$ is given by Eq.(15) and the peak frequency is $\omega_{\text{peak}} \sim \omega_c \sim \gamma^3 c/\rho$; (2) If the bunch is one-dimensional, $P_A(\omega)$ is given by Eq.(16) and the peak frequency is $\omega_{\text{peak}} \sim \omega_l \sim 2c/l$; (3) If the bunch is a bunch-cavity system, $P_A(\omega)$ is given by Eq.(18) and the peak frequency is $\omega_{\text{peak}} \sim \omega_c$.

If one observes a non-white-noise signal in the frequency domain, i.e., $(S/N)_{\text{peak}} \gg 1$, $\lambda_b \gg \omega_{\text{peak}}$ is required. For the GHz signal with $\omega_{\text{peak}}/2\pi \sim 10^9$ rad s^{-1} , the bunch formation rate should be $\lambda_b \gg 10^9 s^{-1}$, leading to $\lambda_B \simeq \lambda_b/2\gamma^2 \gtrsim 10^3 s^{-1} \gamma_3^{-2}$. In particular, for an FRB with a typical duration of a few milliseconds, at least one bunch is produced during $\Delta t \sim 1$ ms, leading to $\lambda_B \gtrsim 1/\Delta t \sim 10^3 s^{-1}$ and $\lambda_b \simeq 2\gamma^2 \lambda_B \gtrsim 10^9 s^{-1} \gamma_3^2 \sim \omega_{\text{peak}}$ and $(S/N)_{\text{peak}} \gtrsim 1$. Thus, the white-noise signal might not be significant for an FRB, if the FRB is produced by the bunch with a Lorentz factor $\gamma \gtrsim 10^3$. Notice that the above conclusion potentially assumes that $\tau_b \lambda_b \ll 1$ for the impulsive sampling profile.

3.2.2 Rectangular sampling profile

Next, we generally consider that the function $s(t)$ given by Eq.(24) could be well described by a rectangular profile with width τ_b , i.e.

$$s(t) = \text{rect}\left(\frac{t}{\tau_b}\right) \equiv \begin{cases} 1 & \text{for } \left| \frac{t}{\tau_b} \right| \leq \frac{1}{2}, \\ 0 & \text{for } \left| \frac{t}{\tau_b} \right| > \frac{1}{2}, \end{cases} \tag{42}$$

where $\text{rect}(x)$ is the rectangular function. Using Eq.(23) and Eq.(29), the autocorrelation function $R_S(\tau)$ is

$$R_S(\tau) = (\lambda_b \tau_b)^2 + \lambda_b \tau_b \Lambda\left(\frac{\tau}{\tau_b}\right), \quad (43)$$

where $\Lambda(x)$ is the triangular function

$$\Lambda(x) \equiv \begin{cases} 1 - |x| & \text{for } |x| \leq 1, \\ 0 & \text{for otherwise.} \end{cases} \quad (44)$$

According to Eq.(36), the emission spectrum of $S(t)$ is

$$P_S(\omega) = (\lambda_b \tau_b)^2 \delta(\omega) + \frac{\lambda_b \tau_b^2}{2\pi} \text{sinc}^2\left(\frac{\tau_b \omega}{2}\right). \quad (45)$$

Using Eq.(35), the emission spectrum of $\tilde{A}(t)$ is

$$P_{\tilde{A}}(\omega) = (\lambda_b \tau_b)^2 P_A(\omega) + \frac{\lambda_b \tau_b^2}{2\pi} P_A(\omega) * \text{sinc}^2\left(\frac{\tau_b \omega}{2}\right). \quad (46)$$

Compared with that of a single persistent bunch, the emission spectrum of a fluctuating bunch is suppressed by a factor of $\sim (\lambda_b \tau_b)^2 = (\lambda_B \tau_B)^2$. The signal-to-noise ratio at the peak frequency in the frequency domain is given by

$$\left. \frac{S}{N} \right|_{\text{peak}} = \frac{2\pi \lambda_b P_A(\omega_{\text{peak}})}{P_A(\omega) * \text{sinc}^2(\tau_b \omega / 2)}. \quad (47)$$

According to the property of the convolution of two pulse profiles, we have the following conclusions: (1) If $\tau_b > \omega_{\text{peak}}^{-1}$, one has $(S/N)_{\text{peak}} \sim \lambda_b \tau_b = \lambda_B \tau_B$, and the cutoff frequency of the whole spectrum is at $\sim \omega_{\text{peak}}$, see the top panel of Figure 5. (2) If $\tau_b < \omega_{\text{peak}}^{-1}$, one has $(S/N)_{\text{peak}} \sim \lambda_b / \omega_{\text{peak}}$, and there is a high-frequency cutoff in the white noise at $\tau_b^{-1} \sim \tilde{\omega}_c$, see the bottom panel of Figure 5. In particular, when $\tau_b \rightarrow 0$, one has $\text{sinc}^2(\tau_b \omega / 2) \sim 1$, so the above results become the case of an impulsive sampling profile as discussed in Section 3.2.1. In summary, for both cases, the cutoff frequency is at

$$\omega_{\text{cut}} \sim \max(\omega_{\text{peak}}, \tau_b^{-1}), \quad (48)$$

and the signal-to-noise ratio at the peak frequency in the frequency domain is

$$\left. \frac{S}{N} \right|_{\text{peak}} \sim \frac{\lambda_b}{\min(\omega_{\text{peak}}, \tau_b^{-1})}. \quad (49)$$

3.3 Radiation by multiple fluctuating bunches along a field line

Next, we discuss the radiation by multiple fluctuating bunches along a field line, that is, there is a bunch train (with more than one bunch) along the field line. Each bunch emits a radiation pulse with the same shape but with random arrival times. We consider that the radiation by the first fluctuating bunch in the bunch train is $\tilde{A}(t)$, then the radiation by multiple fluctuating bunches could be described as

$$\hat{A}(t) = \sum_j^N \tilde{A}(t - t_j), \quad (50)$$

where t_j is the arrival time of the pulse generated by the j -th bunch, and N is the total number of bunches along a field line. Similar to the generation process of a bunch that has been considered to be a Poisson process as discussed above, the distribution of multiple fluctuating bunches along a field line may also satisfy the Poisson process, i.e., $\{t_j\}$ satisfies

$$p_{t_j}(t) = \lambda_T P_{j-1}(t), \quad (51)$$

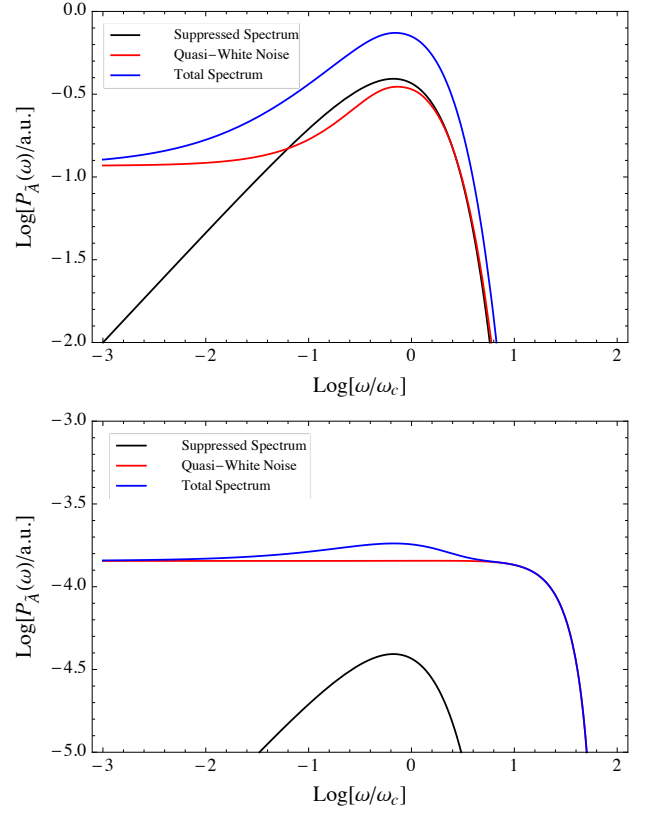


Figure 5. The emission spectrum of a single fluctuating bunch. The black, red, and blue curves correspond to the suppressed emission spectrum $(\lambda_b \tau_b)^2 P_A(\omega)$, the quasi-white noise $(\lambda_b \tau_b^2 / 2\pi) P_A(\omega) * \text{sinc}^2(\tau_b \omega / 2)$, and the total emission spectrum, respectively. The top panel is the case with $\lambda_b = 0.1 \omega_{\text{peak}}$ and $\tau_b = 10 \omega_{\text{peak}}^{-1}$, and the bottom panel is the case with $\lambda_b = 0.1 \omega_{\text{peak}}$ and $\tau_b = 0.1 \omega_{\text{peak}}^{-1}$. Here we take $P_A(\omega)$ as the emission spectrum of a single persistent source given by Eq.(15) and the peak frequency is $\omega_{\text{peak}} = \omega_c$. The unit of the emission spectrum is arbitrary.

where λ_T^{-1} corresponds to the average time separation between two adjacent bunches.

According to the time shifting property of Fourier transform, $\mathcal{F}[\tilde{A}(t - t_j)] = e^{i\omega t_j} \tilde{A}(\omega)$, the Fourier transform of $\hat{A}(t)$ is

$$\hat{A}(\omega) = \mathcal{F}[\hat{A}(t)] = \tilde{A}(\omega) \sum_j^N e^{i\omega t_j}. \quad (52)$$

Therefore, the emission spectrum of multiple fluctuating bunches is

$$P_{\hat{A}}(\omega) = 2|\hat{A}(\omega)|^2 = P_{\tilde{A}}(\omega) \left| \sum_j^N e^{i\omega t_j} \right|^2. \quad (53)$$

The coherence properties of the radiation by the bunch train are determined by the factor of $|\sum_j^N e^{i\omega t_j}|^2$, and we will summarize its characteristics as follows: (1) If the bunch separation is much larger than the wavelength, i.e., $\omega(t_j - t_{j-1}) \sim \omega \lambda_T^{-1} \gg 2\pi$, the phase factor $e^{i\omega t_j}$ would be randomly distributed in the complex number plane, leading to

$$P_{\hat{A}}(\omega) = P_{\tilde{A}}(\omega) \left(N + \sum_{j \neq k} \sum e^{i\omega(t_j - t_k)} \right) \simeq N P_{\tilde{A}}(\omega), \quad (54)$$

where $\sum_{j \neq k} e^{i\omega(t_j - t_k)} \simeq 0$, because $\omega(t_j - t_k)$ are randomly distributed in $[0, 2\pi]$. In this case, the radiation by multiple fluctuating

bunches is the incoherent sum of those of many single fluctuating bunches, and the spectral shape of $P_{\hat{A}}(\omega)$ is the same as that of $P_{\bar{A}}(\omega)$. (2) If the bunch separation is much smaller than the wavelength, i.e., $\omega(t_j - t_{j-1}) \sim \omega\lambda_T^{-1} \ll 2\pi$, the sum in Eq.(53) could be approximately calculated via the integration in the complex number plane,

$$\begin{aligned} \left| \sum_j^N e^{i\omega t_j} \right|^2 &\simeq \left| \lambda_T \int_0^T e^{i\omega t} dt \right|^2 = N^2 \left| \frac{e^{i\omega T} - 1}{i\omega T} \right|^2 \\ &= N^2 \left[\frac{\sin(\omega/\omega_T)}{(\omega/\omega_T)} \right]^2 \quad \text{with } \omega_T = \frac{2}{T} = \frac{2\lambda_T}{N}, \end{aligned} \quad (55)$$

where $T = N/\lambda_T$ is the bunch train duration (i.e., the duration time between the first bunch and the last bunch along a field line). One should note that the above equation gives $|\sum_j^N e^{i\omega t_j}|^2 = 0$ when $\omega/\omega_T = n\pi$ with $n \in \mathbb{Z}^+$. The result of zero is due to the homogeneity and continuity assumptions in the integration calculation. The random process involved here will cause $|\sum_j^N e^{i\omega t_j}|^2 \sim N$ when $\omega/\omega_T = n\pi$. A Monte Carlo simulation with a distribution of Eq.(51) could be used to test this result. Thus, the emission spectrum of multiple fluctuating bunches is

$$P_{\hat{A}}(\omega) \simeq \max \left[N^2 \text{sinc}^2 \left(\frac{\omega}{\omega_T} \right), N \right] P_{\bar{A}}(\omega). \quad (56)$$

According to Eq.(56), the emission spectrum will become completely incoherent (N term in the max function is dominated) for $\omega \gg 2\lambda_T/\sqrt{N}$, meanwhile, Eq.(56) is also applicable to Eq.(54) in the case (1) due to $N \gg 1$. Furthermore, if the total bunch train length is much smaller than the wavelength, i.e., $\omega T \ll 1$, one has $|\sum_j^N e^{i\omega t_j}|^2 \sim N^2$, leading to

$$P_{\hat{A}}(\omega) \simeq N^2 P_{\bar{A}}(\omega). \quad (57)$$

The emission from the bunch train is significantly coherent in this case. In Figure 6, we plot the radiation spectrum of the multiple fluctuating bunches with different values of λ_T based on Eq.(56). We can see the radiation is coherent for $\omega \lesssim 2\lambda_T/\sqrt{N}$ and incoherent for $\omega \gtrsim 2\lambda_T/\sqrt{N}$.

4 FORMATION AND DISPERSION OF FLUCTUATING BUNCHES

The above treatment has assumed continuous generation and dispersion of bunches. In this section, we discuss some mechanisms to produce bunches discussed in the literature.

In the magnetosphere of a neutron star, charged bunches could be generated by the development of a two-stream instability in a non-stationary plasma. For a pair plasma, there are three possible ways by which a two-stream instability can develop in the magnetosphere: (1) The two-stream instability is driven by the interaction between a high-energy beam and a secondary pair plasma (Ruderman & Sutherland 1975; Benford & Buschauer 1977). Such a mechanism is known to be inefficient; (2) The two-stream instability is due to the longitudinal drift of electrons and positrons in the secondary pair plasma (Cheng & Ruderman 1977); (3) The two-stream instability is produced by the overlapping secondary plasma clouds with different velocities due to intermittent discharges at the polar gap (Usov 1987; Usov & Usov 1988).

The two-stream instability leads to the formation of electrostatic Langmuir waves. When a Langmuir wave propagates in the magnetosphere, the oscillating electric field of the Langmuir wave forms

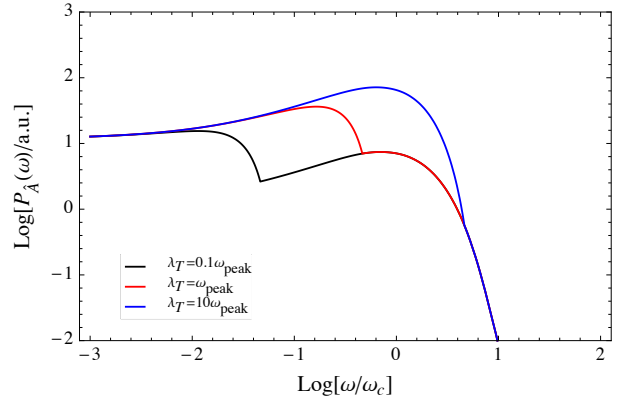


Figure 6. The emission spectrum of multiple fluctuating bunches. The black, red, and blue curves correspond to the cases with $\lambda_T = 0.1\omega_{\text{peak}}$, $\lambda_T = \omega_{\text{peak}}$ and $\lambda_T = 10\omega_{\text{peak}}$, respectively. Here we take $P_{\bar{A}}(\omega)$ as the emission spectrum of a fluctuating bunch given by Eq.(46) (the corresponding emission spectrum $P_A(\omega)$ of the single persistent source is given by Eq.(15)). The peak frequency is $\omega_{\text{peak}} = \omega_c$. $\lambda_b = 0.1\omega_{\text{peak}}$ and $\tau_b = 10\omega_{\text{peak}}^{-1}$ are taken. The unit of the emission spectrum is arbitrary. For clear display, we take the bunch number as $N = 10$ in this figure. A larger value of N would make the emission spectrum difference between the low-frequency coherent component and the high-frequency component more significant, and the break frequency is at $\sim 2\lambda_T/\sqrt{N}$.

a longitudinal concentration of charges, i.e., charged bunches. However, the formation of charge bunches capable of explaining coherent radio emission has the following fundamental difficulty (Lominadze et al. 1986; Melikidze et al. 2000; Lakoba et al. 2018). On one hand, the typical length l of a bunch should be smaller than half of the wavelength $\lambda/2$ of the electromagnetic wave, $l < \lambda/2$, which makes the coherent radiation significant; otherwise, different regions in the bunch would emit independently and hence incoherently (see also Section 3.1 for the effect by the bunch length). Meanwhile, if the bunches are caused by linear Langmuir waves with a wavelength λ_L , the bunch size is about half of the wavelength of the Langmuir wave, $l \sim \lambda_L/2$. Thus, the coherence condition is $\lambda > \lambda_L$, leading to

$$\omega < \omega_L, \quad (58)$$

where the approximate dispersion relations of $\omega \simeq kc$ and $\omega_L \simeq kL_c$ are considered here.

On the other hand, the timescale of the radiative process, $2\gamma^2\omega_{\text{cr}}^{-1}$, where $\omega_{\text{cr}} = \omega_c$ or $\tilde{\omega}_c$ is the typical frequency corresponding to the radiation process, must be shorter than the timescale τ_B over which the bunch exists. The bunch lifetime τ_B can be estimated as follows: the bunch lifetime in the plasma rest frame corresponds to the half of the period of the plasma oscillation, $\tau'_B \sim \pi\gamma^{1/2}\omega_p^{-1}$, where ω_p is the plasma frequency in the observer frame, and the factor of $\gamma^{1/2}$ is attributed to the density compression in the Lorentz transformation. In the observer frame, the bunch's lifetime is

$$\tau_B \sim \gamma\tau'_B \sim \pi\gamma^{3/2}\omega_p^{-1} \sim 2\pi\gamma^2\omega_L^{-1}, \quad (59)$$

where $\omega_L \sim 2\gamma^{1/2}\omega_p$ is the Langmuir wave frequency², see the following discussion. Thus, this condition approximately requires $\omega_{\text{cr}} \gtrsim \omega_L$. If the observed frequency is mainly at $\omega \sim \omega_{\text{cr}}$, one

² Note that the Langmuir wave frequency ω_L describes the wave oscillation frequency at a certain spatial position that does not directly reflect the bunch lifetime in the observer frame.

finally has

$$\omega \gtrsim \omega_L. \quad (60)$$

The above two conditions of Eq.(58) and Eq.(60) are in contradiction with each other. Thus, the bunches created by the linear Langmuir wave cannot be a possible source of coherent curvature radiation.

There might be some solutions to break the conditions of Eq.(58) and Eq.(60): (1) The charged bunches, such as ‘‘charged solitons’’ proposed by Melikidze et al. (2000), might exist for a duration much longer than the plasma oscillation period; (2) The bunch length is no longer related to the half-wavelength of Langmuir wave due to the non-linear effects; (3) The observed frequency ω is much smaller than the typical frequency ω_{cr} that corresponds to the radiation process, $\omega \ll \omega_{cr}$. In the last case, the observed frequency ω is no longer directly related to the radiative process, leading to both $\omega < \omega_L$ and $\omega_{cr} \gtrsim \omega_L$ satisfied simultaneously (but there might be a possible absorption in the low-frequency band).

For the first two solutions, a non-linear Langmuir wave is preferred to produce the charged bunches contributing to significant coherent radio emission (e.g., Melikidze et al. 2000; Lakoba et al. 2018; Rahaman et al. 2022). The non-linear theory usually requires a priori a large amplitude for the Langmuir waves, i.e., the growth rate is sufficient for the breakdown of the linear theory (e.g., Rahaman et al. 2020).

We consider that the α -th species in the plasma has the number density n_α , charge q_α , mass m_α , dimensionless momenta p_α , and equilibrium distribution function $f_\alpha^{(0)}$. The dispersion relation of the Langmuir wave of a one-dimensional relativistic plasma flow is given by (e.g., Gedalin et al. 2002; Asseo & Melikidze 1998; Rahaman et al. 2020)

$$1 - \sum_\alpha \omega_{p,\alpha}^2 \int \frac{1}{\gamma_\alpha^3} \frac{f_\alpha^{(0)}}{(\omega - \beta_\alpha kc)^2} dp_\alpha = 0, \quad (61)$$

where $\omega_{p,\alpha} = (4\pi q_\alpha^2 n_\alpha / m_\alpha)^{1/2}$ is the plasma frequency, and $\gamma_\alpha = (1 + p_\alpha^2)^{1/2}$ is the Lorentz factor and $\beta_\alpha = p_\alpha / \gamma_\alpha$ is the dimensionless velocity. The cut-off frequency of the Langmuir waves corresponds to the long wavelength limit $k \rightarrow 0$, leading to

$$\omega_{cut}^2 = \sum_\alpha \omega_{p,\alpha}^2 \int \frac{f_\alpha^{(0)}}{\gamma_\alpha^3} dp_\alpha, \quad (62)$$

and the characteristic frequency corresponds to the Langmuir mode touching the $\omega = kc$ line, leading to

$$\omega_L^2 = \sum_\alpha \omega_{p,\alpha}^2 \int \frac{1}{\gamma_\alpha^3} \frac{f_\alpha^{(0)}}{(1 - \beta_\alpha)^2} dp_\alpha. \quad (63)$$

We note that the Langmuir waves cannot exist for $\omega_{cut} < \omega < \omega_L$ (superluminal waves), because the phase velocity of the Langmuir wave exceeds the light speed. If $\omega > \omega_L$ (subluminal waves), the phase velocity of the Langmuir wave is smaller than the light speed, which can cause the development of two-stream instability. For example, if the distribution function of the pair plasma is close to a Gaussian distribution with a center of γ_\pm and spread of $\Delta\gamma_\pm \ll \gamma_\pm$, i.e., the distribution function can be approximately described by the delta-function at γ_\pm , i.e., $f_\pm^{(0)} \sim \delta(p - p_\pm)$. The above two typical frequencies would become $\omega_{cut} \sim \gamma_\pm^{-3/2} \omega_{p,\pm}$ and $\omega_L \sim 2\gamma_\pm^{1/2} \omega_{p,\pm}$, where $\omega_\pm = (4\pi e^2 n_\pm / m_e)^{1/2}$ is the pair plasma frequency, and n_\pm is the number density of the pair plasma.

Since the non-linear theory usually requires that the growth rate is sufficient for the breakdown of the linear theory, we first discuss the growth rate of two-stream instability by linear waves. We consider

that there are two plasma components (that are denoted by ‘‘1’’ and ‘‘2’’) with a relative motion along the magnetic field line. Their typical Lorentz factors are γ_1 and γ_2 with $\gamma_1 \gg \gamma_2$, and their number densities are n_1 and n_2 , respectively. In the rest frame of each component, the plasma is assumed to be cold (the treatment for instability in a hot plasma could be seen in the recent work of Rahaman et al. (2020); Melrose et al. (2021)), leading to $f_j^{(0)} \simeq \delta(p - p_j)$ with $j = 1, 2$. According to Eq.(61), the dispersion relation can be written as

$$1 - \frac{\omega_{p,1}^2}{\gamma_1^3 (\omega - \beta_1 kc)^2} - \frac{\omega_{p,2}^2}{\gamma_2^3 (\omega - \beta_2 kc)^2} = 0, \quad (64)$$

where $\omega_{p,j} = (4\pi e n_j / m_e)^{1/2}$ is the plasma frequency of the component j . We consider the resonant reactive instability as the bunching mechanism (the discussion for the non-resonant reactive instability and kinetic instability could be seen in Gedalin et al. (2002); Rafat et al. (2019); Rahaman et al. (2020)). The solution of the above equation gives the growth rate (e.g., Usov 1987; Gedalin et al. 2002)

$$\Gamma \sim \gamma_1^{-1} \gamma_2^{-1} \left(\frac{n_1}{n_2} \right)^{1/3} \omega_L, \quad (65)$$

and the characteristic frequency of the Langmuir wave is

$$\omega_L \sim 2\gamma_2^{1/2} \omega_{p,2}, \quad (66)$$

In the following discussion, we analyze the bunch formation condition according to these results.

The amplitude of the linear Langmuir wave triggered by the two-stream instability depends on the gain

$$G = \Gamma \Delta t = \Gamma \frac{\Delta r}{c} \sim \Gamma \frac{r}{c}, \quad (67)$$

where $\Delta t = \Delta r / c$ is the time available for the growth, and Δr is the distance available for the growth along the field line. The Langmuir wave amplitude is $\propto e^G$. In the magnetic field, the plasma density satisfies $n \propto r^{-m}$, where $m = 3, 4$ corresponds to the Goldreich-Julian magnetosphere (Goldreich & Julian 1969) and the twisted magnetosphere, respectively (also see the following discussion). Thus, $n_1/n_2 \sim \text{const}$ and $\omega_{p,2} \propto r^{-3/2}$ or r^{-2} in Eq.(65). The typical distance for the variation of the linear growth rate is $\Delta r \sim (2/3)r$ or $(1/2)r$ for $\Delta\omega_{p,2} \sim \omega_{p,2}$. We approximately take $G \sim \Gamma r / c$.

The non-linear theory requires a large amplitude of the Langmuir waves. Rahaman et al. (2020) proposed the following condition to indicate the breakdown of the linear theory: if the field energy density is equal to the total energy density, the linear theory would break down. Based on the energy distribution among Langmuir waves and particles in the plasma, Rahaman et al. (2020) obtained a threshold gain indicating the breakdown of the linear regime,

$$G_{th} \simeq \frac{1}{2} \ln \sum_\alpha \gamma_\alpha^2. \quad (68)$$

Due to the logarithmic function in the above equation, the typical value of the gain threshold for the two-stream instability in various scenarios in the magnetosphere is about $G_{th} \sim \text{a few}$.

The sufficient amplification would drive the system beyond the linear regime when $G = G_{th}$, and the charged bunches contributing to significant coherent radio emission could be produced by the non-linear wave further. Thus, the bunch formation rate can be written as

$$\lambda_B \sim \Gamma(G = G_{th}), \quad (69)$$

and the bunch separation $l_T = c\lambda_T^{-1}$ corresponds to the wavelength of the Langmuir wave when $G \simeq G_{\text{th}}$, i.e.

$$l_T \equiv \frac{c}{\lambda_T} = \frac{2\pi c}{\omega_L} \sim \frac{\pi c}{\gamma_2^{1/2} \omega_{p,2}} \quad (70)$$

according to Eq.(66). Due to the non-linear effect, the bunch size and lifetime would not be directly related to the Langmuir wave. For example, the charged solitons proposed by [Melikidze et al. \(2000\)](#) could exist for a time much longer than the period of the Langmuir wave and the typical ripple size in one charged soliton also depends on the detailed properties of the soliton ([Melikidze et al. 2000](#); [Lakoba et al. 2018](#); [Rahaman et al. 2022](#)). Here, we briefly involve two parameters (ζ_l, ζ_τ) attributed to the non-linear effect to correct the bunch size l and lifetime τ_B ,

$$l = \zeta_l \frac{2\pi c}{\omega_L} \sim \frac{\pi c \zeta_l}{\gamma_2^{1/2} \omega_{p,2}}, \quad (71)$$

$$\tau_B = \zeta_\tau \frac{2\pi \gamma^2}{\omega_L} \sim \frac{\gamma_2^{3/2} \pi \zeta_\tau}{\omega_{p,2}}, \quad (72)$$

where the factor of γ^2 in τ_B is attributed to Eq. (59).

Based on the above theory, as an example, we consider that the development of a two-stream instability is due to the non-stationarity of the plasma stream, and the pair plasma that flows out from the pulsar is inhomogeneous and gathers into separate clouds along the field lines ([Usov 1987](#); [Ursov & Usov 1988](#); [Asseo & Melikidze 1998](#)). The Lorentz factors of the electrons/positrons in the pair plasma have a distribution ranging from γ_{\min} to γ_{\max} , so the pair clouds disperse as they flow out from the neutron star. The energy distribution of the plasma particles satisfies

$$n(\gamma)d\gamma = n_\gamma \gamma^{-p} d\gamma \quad (73)$$

with $n_\gamma \equiv (p-1)\gamma_{\min}^{p-1} n_\pm$, where n_\pm is the total pair number density. At the interaction distance r_i , the high-energy particles with $\gamma \sim \gamma_{\max}$ of the cloud B catch up with the low-energy particles with $\gamma \sim \gamma_{\min}$ of the cloud A in front of the cloud B with an initial separation L . The interaction distance is

$$r_i = \frac{L}{v_{\max} - v_{\min}} \simeq 2\gamma_{\min}^2 L \quad (74)$$

for $\gamma_{\max} \gg \gamma_{\min} \gg 1$, where v_{\min} and v_{\max} are the particle minimum and maximum velocities, respectively. Here we briefly assume that cloud A and B have the same number density.

At the distance r_i , there are approximately only particles with $\gamma \sim \gamma_{\min}$ and $\gamma \sim \gamma_{\max}$ in the merged cloud, so the two-stream instability could develop. Component 1 has a density $\sim \gamma_{\max} n(\gamma_{\max})$ and Lorentz factor γ_{\max} , and Component 2 has a density $\sim \gamma_{\min} n(\gamma_{\min})$ and Lorentz factor γ_{\min} . According to Eq.(65) and Eq.(73), the growth rate of the two-stream instability is

$$\Gamma \sim \gamma_{\min}^{\frac{2p-5}{6}} \gamma_{\max}^{-\frac{p+2}{3}} \omega_p, \quad (75)$$

where $\omega_p = (4\pi n_e/m_e)^{1/2}$ and $n_e \sim \gamma_{\min} n(\gamma_{\min})$. In the magnetosphere, the pair plasma density is approximately given by

$$n_\pm \sim \kappa \max(n_{\text{GJ}}, n_{\text{twist}}) \simeq \kappa \max\left(\frac{\Omega B(r)}{2\pi e c}, \frac{B(r) \sin^2 \theta \Delta\phi}{4\pi e r}\right). \quad (76)$$

where κ is the multiplicity of pair production, $n_{\text{GJ}} = \Omega B(r)/2\pi e c$ is the Goldreich-Julian density ([Goldreich & Julian 1969](#)), $n_{\text{twist}} = \nabla \times \vec{B}/4\pi e \sim B(r) \sin^2 \theta \Delta\phi/4\pi e r$ is the net charge number density in a twisted magnetosphere, $B(r) = B_p (r/R_n)^{-3}$ is the strength of a dipole field at the distance r , B_p is the surface magnetic field, R_n is

the neutron star radius, and Ω is the neutron star angular velocity, θ is the poloidal angle and $\Delta\phi$ is the twisting angle of the field.

For example, we consider that a magnetar has a surface magnetic field $B_p \sim 10^{14}$ G, a rotation period $P \sim 0.1$ s, a twisting angle $\Delta\phi \sim 0.1$ rad, a polar angle $\sin^2 \theta \sim 0.1$, a multiplicity $\kappa \sim 10^3$, and an outflowing plasma Lorentz factor $\gamma_\pm \sim 100$. Because $n_{\text{twisting}} \gg n_{\text{GJ}}$ for the above typical parameters, the pair number density is $n_\pm \sim 1.6 \times 10^9 \text{ cm}^{-3} r_8^{-4}$ and $n_e \sim \gamma_{\min} n(\gamma_{\min}) \sim n_\pm$. We take $\gamma_{\min} \sim \gamma_\pm \sim 100$, $\gamma_{\max} \sim 10^4$ and $p \sim 2.5$. Thus, the linear growth rate for the development of the two-stream instability is $\Gamma \sim 2.3 \times 10^3 \text{ s}^{-1} r_8^{-2}$. Therefore, the non-linear Langmuir wave develops at $r \sim 7.6 \times 10^8 \text{ cm}$ where $G \sim G_{\text{th}} \sim O(1)$ is satisfied, and the correspond bunch formation rate is $\lambda_B \sim 40 \text{ s}^{-1}$. The bunch separation is $l_T \sim \pi c/\gamma_\pm^{1/2} \omega_p \sim 240 \text{ cm}$, and the bunch size and lifetime might be $l \sim 24 \text{ cm}$, $\zeta_{l,-1}$ and $\tau_B \sim 7.9 \times 10^{-3} \text{ s}$, $\zeta_{\tau,2}$, respectively. Charged bunches capable of contributing to coherent radio emission must be long-lived as proposed by [Melikidze et al. \(2000\)](#); [Rahaman et al. \(2022\)](#).

5 CONCLUSIONS AND DISCUSSIONS

Although coherent curvature radiation by charged bunches has been proposed to explain the coherent emissions of radio pulsars and FRBs, this mechanism still encounters some issues, including how the charged bunches form and disperse and what the radiation features are for the case of fluctuating bunches in the emission region. In this work, we consider that the bunches in a neutron star magnetosphere form with an average rate of λ_B and have an average lifetime of τ_B . We mainly analyze the spectral features of coherent curvature radiation by dynamically fluctuating bunches and discuss the possible physical mechanism for the formation and dispersion of the charged bunches in the magnetosphere of a neutron star. The following conclusions are drawn:

1. We first point out that the classical formula of calculating the brightness temperature of FRB emission, i.e. Eq.(1), that involves the transient duration Δt is not applicable to the scenario of the magnetospheric curvature radiation, because Δt does not directly reflect the transverse size l_e of the emission region for curvature radiation. Considering that the charged bunches move along the field line with a Lorentz factor γ at a distance r from the neutron star center, the transverse size of the emission region is estimated as $l_e \sim r/\gamma$ for $\omega \sim \omega_c$, leading to $l_e \ll c\Delta t$. Therefore, for the typical parameters of the magnetosphere, the brightness temperature should be much larger than that given by Eq.(1).

2. The classical theory of curvature radiation potentially assumes that the bunch lifetime satisfies $\tau_B > \rho/\gamma c$, where ρ is the curvature radius and γ is the bunch Lorentz factor. Both the typical frequency and the cutoff frequency are $\omega_c \sim \gamma^3 c/\rho$ and the spectral feature depends on the spatial structure of the bunch. For example, we consider that the bunch has a lengthscale of l . Compared with the radiation spectrum of a single point-charge persistent bunch, the radiation spectrum by an extending bunch is corrected by a factor of $\text{sinc}^2(\omega/\omega_l)$ with $\omega_l \sim 2c/l$, and the radiation power is suppressed by a factor of $(\omega_l/\omega_c)^{5/3}$. In particular, since the excess of one charge is usually compensated by the lack of this charge in the nearby regions, a bunch-cavity system might form in the magnetosphere. It has an emission spectrum much narrower than that of a single persistent bunch and with the emission spectrum of $P_A(\omega) \propto \omega^{8/3}$ in the low-frequency band.

3. If the bunch lifetime is short enough, $\tau_B < \rho/\gamma c$, the cutoff

frequency would become $\tilde{\omega}_c \sim \gamma^2/\tau_B \gtrsim \omega_c$. Thus, a short-lived bunch will radiate electromagnetic waves with a higher frequency compared with that of classical curvature radiation. Considering that bunches form and disperse intermittently when the building plasma particles move along a magnetic field line, the emission spectrum of such a fluctuating bunch is a convolution between the emission spectrum of a single persistent bunch $P_A(\omega)$ and that of the pulse sampling function $P_S(\omega)$, $P_{\tilde{A}}(\omega) = P_A(\omega) * P_S(\omega)$, where $P_S(\omega)$ is the emission spectrum of the pulse sampling function $S(t)$ that is described by Eq. (23) and Figure 4.

4. According to the above point, we obtained the emission spectrum of a single fluctuating bunch, $P_{\tilde{A}}(\omega)$. We find that compared with that of a single fluctuating bunch, $P_{\tilde{A}}(\omega)$ is suppressed by a factor of $(\lambda_b \tau_b)^2$, where $\lambda_b \simeq 2\gamma^2 \lambda_B$ and $\tau_b \simeq \tau_B/2\gamma^2$ are the pulse rate and duration, respectively, λ_B and τ_B are the bunch formation rate and lifetime, respectively, and the factor of $2\gamma^2$ is corrected by the propagation time-delay effect. Meanwhile, there is a quasi-white noise in the wider band. We define $(S/N)_{\text{peak}}$ as the ‘‘signal-to-noise ratio’’ at the peak frequency ω_{peak} in the frequency domain, and $(S/N)_{\text{peak}} \gtrsim 1$ means that the spectrum is non-white-noise. If $\tau_b < \omega_{\text{peak}}^{-1}$, one has $(S/N)_{\text{peak}} \sim \lambda_b/\omega_{\text{peak}}$, and there is a high-frequency cutoff in the white noise at $\tau_b^{-1} \sim \tilde{\omega}_c$. If $\tau_b > \omega_{\text{peak}}^{-1}$, one has $(S/N)_{\text{peak}} \sim \lambda_b \tau_b = \lambda_B \tau_B$, the cutoff frequency of the whole spectrum is at $\sim \omega_{\text{peak}}$.

5. For multiple fluctuating bunches along a field line, if the bunch separation is longer than the wavelength, the emission spectrum of multiple fluctuating bunches would be the incoherent summation of that of each single fluctuating bunch. On the other hand, if the bunch separation is much smaller than the wavelength, the coherent radiation by multiple fluctuating bunches could be described by Eq.(56), suggesting that the total radiation power is at least larger than the incoherent value.

At last, we also notice that the theory of the spectral analysis for fluctuating bunches not only applies to curvature radiation but also to coherent inverse Compton scattering (ICS) by charged bunches (Zhang 2022b). This mechanism generally has a much higher radiation power than curvature radiation, so that a lower degree of coherence is needed to interpret FRBs. Similar to the scenario of curvature radiation, a white-noise component in the emission spectrum would also appear due to bunch fluctuations. Compared with coherent curvature radiation, the major difference is that the emission spectrum of coherent ICS mainly depends on the properties of the incident electromagnetic waves which should be involved in the discussion of the emission of a single persistent bunch. On the other hand, since the radiation direction of coherent ICS is also along the magnetic field line due to the relativistic motion of the bunches, its emission spectrum might be modulated by the typical frequency ω_c . A detailed analysis of this mechanism will be performed in the future.

ACKNOWLEDGEMENTS

We thank the anonymous referee for the helpful comments and suggestions. We also thank Qiao-Chu Li for the constructive discussion about the signal theory and acknowledge helpful discussions with Ze-Nan Liu, Mordehai Milgrom and Yue Wu. Y-PY’s work is supported by the National Natural Science Foundation of China grant No.12003028, the National SKA Program of China (2022SKA0130100), and the China Manned Space Project (CMS-CSST-2021-B11).

DATA AVAILABILITY

This theoretical study did not generate any new data.

REFERENCES

- Asseo E., Melikidze G. I., 1998, *MNRAS*, 301, 59
 Bailes M., 2022, *Science*, 378, abj3043
 Basu R., Mitra D., Melikidze G. I., 2022, *ApJ*, 927, 208
 Beloborodov A. M., 2017, *ApJ*, 843, L26
 Benford G., Buschauer R., 1977, *MNRAS*, 179, 189
 Buschauer R., Benford G., 1976, *MNRAS*, 177, 109
 Cheng A. F., Ruderman M. A., 1977, *ApJ*, 212, 800
 Cooper A. J., Wijers R. A. M. J., 2021, *MNRAS*, 508, L32
 Cordes J. M., Chatterjee S., 2019, *ARA&A*, 57, 417
 Franks L. E., 1981, *Signal Theory (Revised Edition)*
 Gedalin M., Gruman E., Melrose D. B., 2002, *MNRAS*, 337, 422
 Gil J., Lyubarsky Y., Melikidze G. I., 2004, *ApJ*, 600, 872
 Ginzburg V. L., Zhelezniakov V. V., 1975, *ARA&A*, 13, 511
 Goldreich P., Julian W. H., 1969, *ApJ*, 157, 869
 Jackson J. D., 1998, *Classical Electrodynamics*, 3rd Edition
 Katz J. I., 2014, *Phys. Rev. D*, 89, 103009
 Katz J. I., 2018, *MNRAS*, 481, 2946
 Kumar P., Bošnjak Ž., 2020, *MNRAS*, 494, 2385
 Kumar P., Lu W., Bhattacharya M., 2017, *MNRAS*, 468, 2726
 Kumar P., Gill R., Lu W., 2022, *MNRAS*, 516, 2697
 Lakoba T., Mitra D., Melikidze G., 2018, *MNRAS*, 480, 4526
 Liu Z.-N., Wang W.-Y., Yang Y.-P., Dai Z.-G., 2022, *arXiv e-prints*, p. arXiv:2212.13153
 Lominadze D. C., Machabeli G. Z., Melikidze G. I., Pataraya A. D., 1986, *Soviet Journal of Plasma Physics*, 12, 712
 Longair M. S., 2011, *High Energy Astrophysics*
 Lu W., Kumar P., 2018, *MNRAS*, 477, 2470
 Lu W., Kumar P., Zhang B., 2020, *MNRAS*, 498, 1397
 Luo J.-W., Zhu-Ge J.-M., Zhang B., 2023, *MNRAS*, 518, 1629
 Lyubarsky Y., 2014, *MNRAS*, 442, L9
 Lyubarsky Y., 2021, *Universe*, 7, 56
 Lyubarsky Y., Ostrovska S., 2016, *ApJ*, 818, 74
 Melikidze G. I., Gil J. A., Pataraya A. D., 2000, *ApJ*, 544, 1081
 Melrose D. B., 2017, *Reviews of Modern Plasma Physics*, 1, 5
 Melrose D. B., Rafat M. Z., Mastrano A., 2021, *MNRAS*, 500, 4530
 Metzger B. D., Berger E., Margalit B., 2017, *ApJ*, 841, 14
 Petroff E., Hessels J. W. T., Lorimer D. R., 2019, *A&ARv*, 27, 4
 Qu Y., Zhang B., Kumar P., 2023, *MNRAS*, 518, 66
 Rafat M. Z., Melrose D. B., Mastrano A., 2019, *Journal of Plasma Physics*, 85, 905850603
 Rahaman S. M., Mitra D., Melikidze G. I., 2020, *MNRAS*, 497, 3953
 Rahaman S. M., Mitra D., Melikidze G. I., Lakoba T., 2022, *MNRAS*, 516, 3715
 Ruderman M., 1971, *Phys. Rev. Lett.*, 27, 1306
 Ruderman M. A., Sutherland P. G., 1975, *ApJ*, 196, 51
 Rybicki G. B., Lightman A. P., 1986, *Radiative Processes in Astrophysics*
 Sturrock P. A., 1971, *ApJ*, 164, 529
 Tong H., Wang H.-G., 2022, *Research in Astronomy and Astrophysics*, 22, 075013
 Ursov V. N., Usov V. V., 1988, *Ap&SS*, 140, 325
 Usov V. V., 1987, *ApJ*, 320, 333
 Wang W.-Y., Jiang J.-C., Lee K., Xu R., Zhang B., 2022a, *MNRAS*, 517, 5080
 Wang W.-Y., Yang Y.-P., Niu C.-H., Xu R., Zhang B., 2022b, *ApJ*, 927, 105
 Xiao D., Dai Z.-G., 2022, *A&A*, 657, L7
 Xiao D., Wang F., Dai Z., 2021, *Science China Physics, Mechanics, and Astronomy*, 64, 249501
 Yang Y.-P., Zhang B., 2018a, *ApJ*, 864, L16
 Yang Y.-P., Zhang B., 2018b, *ApJ*, 868, 31
 Yang Y.-P., Zhang B., 2020, *ApJ*, 892, L10
 Yang Y.-P., Zhu J.-P., Zhang B., Wu X.-F., 2020, *ApJ*, 901, L13
 Zhang B., 2020, *Nature*, 587, 45

Zhang B., 2022a, [arXiv e-prints](#), p. [arXiv:2212.03972](#)

Zhang B., 2022b, [ApJ](#), **925**, 53

Zhu-Ge J.-M., Luo J.-W., Zhang B., 2023, [MNRAS](#), **519**, 1823

This paper has been typeset from a \TeX/L\AA\TeX file prepared by the author.